GEOPHYSICAL RESEARCH LETTERS, VOL. 35, L18808, doi:10.1029/2008GL034031, 2008

Emissions of CH_4 and N_2O over the United States and Canada based on a receptor-oriented modeling framework and COBRA-NA atmospheric observations

Eric A. Kort,[1] Janusz Eluszkiewicz,[2] Britton B. Stephens,[3] John B. Miller,[4,5] Christoph Gerbig,[6] Thomas Nehrkorn,[2] Bruce C. Daube,[1] Jed O. Kaplan,[7] Sander Houweling,[8] and Steven C. Wofsy[1]

Received 17 March 2008; revised 9 July 2008; accepted 22 August 2008; published 26 September 2008.

[1] We present top-down emission constraints for two non-CO_2 greenhouse gases in large areas of the U.S. and southern Canada during early summer. Collocated airborne measurements of methane and nitrous oxide acquired during the COBRA-NA campaign in May–June 2003, analyzed using a receptor-oriented Lagrangian particle dispersion model, provide robust validation of independent bottom-up emission estimates from the EDGAR and GEIA inventories. We find that the EDGAR CH_4 emission rates are slightly low by a factor of 1.08 ± 0.15 (2σ), while both EDGAR and GEIA N_2O emissions are significantly too low, by factors of 2.62 ± 0.50 and 3.05 ± 0.61, respectively, for this region. Potential footprint bias may expand the statistically retrieved uncertainties. Seasonality of agricultural N_2O emissions may help explain the discrepancy. Total anthropogenic U.S. and Canadian emissions would be 49 Tg CH_4 and 4.3 Tg N_2O annually, if these inventory scaling factors applied to all of North America. **Citation:** Kort, E. A., J. Eluszkiewicz, B. B. Stephens, J. B. Miller, C. Gerbig, T. Nehrkorn, B. C. Daube, J. O. Kaplan, S. Houweling, and S. C. Wofsy (2008), Emissions of CH_4 and N_2O over the United States and Canada based on a receptor-oriented modeling framework and COBRA-NA atmospheric observations, *Geophys. Res. Lett.*, *35*, L18808, doi:10.1029/2008GL034031.

1. Introduction

[2] Knowledge of greenhouse gas emissions is central to understanding the Earth's climate system. Though CO_2 is the single most important anthropogenic greenhouse gas, non-CO_2 anthropogenic greenhouse gases play a significant role in the Earth's energy balance, contributing nearly as much to radiative forcing (RF) as carbon dioxide (0.977 W m^{-2} compared to 1.626 W m^{-2} in 2004) [*Hofmann et al.*, 2006]. Of non-CO_2 anthropogenic greenhouse gases, CH_4 has the largest RF, while N_2O has the third-largest RF [*Hofmann et al.*, 2006].

[3] Recently, increased attention has been focused on assessing CH_4 sources. Global atmospheric inversions [*Bergamaschi et al.*, 2007; *Chen and Prinn*, 2006] and global emissions sensitivity tests [*Houweling et al.*, 2006] have begun to tighten atmospheric constraints on CH_4 sources, though capabilities are limited on a regional (10^4 km^2–10^6 km^2) scale due reliance on data from remote sites and coarse meteorological resolution (typically $1° \times 1°$ or larger). These shortcomings can be overcome using a regionally focused approach, as taken in the Amazon by *Miller et al.* [2007]. Global studies of N_2O have focused on agricultural and industrial emissions from seasonal to interannual time scales [*Nevison et al.*, 2007; *Hirsch et al.*, 2006; *Prinn et al.*, 1990], but have not attempted to place strong constraints on regional budgets.

[4] In this paper, we constrain emissions of CH_4 and N_2O over large areas of the U.S. and southern Canada using models and data specifically designed to address regional scales at high spatial and temporal resolution. We employ a Lagrangian particle diffusion model (LPDM) to directly connect atmospheric measurements with surface fluxes in a receptor-oriented framework. Our measurements consist of flask samples collected during the CO_2 Boundary Layer Regional Airborne–North America (COBRA-NA) campaign in May and June 2003. A direct comparison of simulations with atmospheric measurements on a fine, regional scale enables us to avoid many of the problems that hamper global inversions, extending methods and applications of LPDMs to regional studies of surface emissions [e.g., *Stohl et al.*, 2003; *Gerbig et al.*, 2003; *Matross et al.*, 2006; *Gimson and Uliasz*, 2003].

2. Study and Measurements

[5] The COBRA-NA campaign consisted of 38 flight legs < 4 hours, from 23 May 2003 through 28 June 2003 (for details see *Hurst et al.* [2006]). Extensive vertical profiling in well-mixed conditions (avoiding frontal and convective activity) was targeted to collect an appropriate data set for assessing surface emissions of measured gases. Locations of the ~300 flasks collected and used in this study, and their collective footprint, can be found in Figure 1. These flasks were analyzed for CO_2, CO, CH_4, H_2, SF_6, and N_2O concentrations, and for O_2/N_2, Ar/N_2, ^{13}C in CO_2, and ^{18}O in CO_2 ratios. The CH_4 and N_2O measurements used

[1]School of Engineering and Applied Sciences and Department of Earth and Planetary Sciences, Harvard University, Cambridge, Massachusetts, USA.
[2]Atmospheric and Environmental Research, Inc., Lexington, Massachusetts, USA.
[3]National Center for Atmospheric Research, Boulder, Colorado, USA.
[4]NOAA Earth System Research Laboratory, Boulder, Colorado, USA.
[5]Also at Cooperative Institute for Research in Environmental Sciences, University of Colorado, Boulder, Colorado, USA.
[6]Max-Planck-Insitut für Biogeochemie, Jena, Germany.
[7]Swiss Federal Institute for Forest, Snow, and Landscape Research, Lausanne, Switzerland.
[8]Netherlands Institute for Space Research and Institute for Marine and Atmospheric Research Utrecht, Utrecht, Netherlands.

0094-8276/08/2008GL034031$05.00

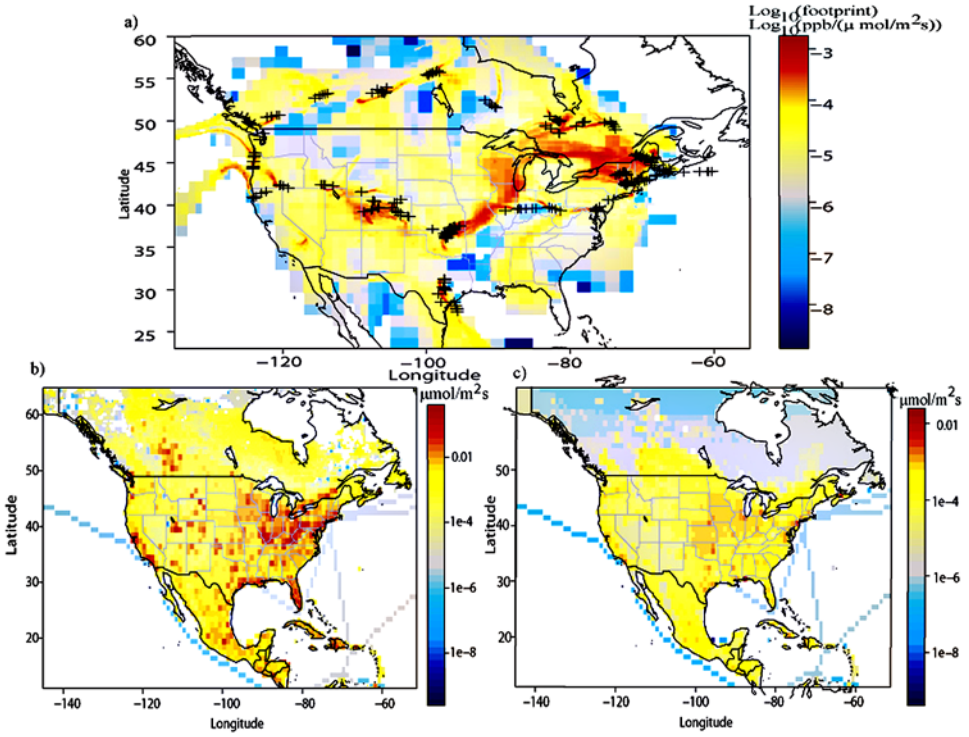

Figure 1. (a) Plus markings indicate locations of airborne flask collection. The average footprint from all the flasks is shown, indicating regions to which our measurements are most sensitive. (b) CH_4 emissions in North America in June (EDGAR and JK). (c) N_2O emissions in North America (EDGAR).

here are calibrated on the NOAA2004 [*Dlugokencky et al.*, 2005] and NOAA2006 [*Hall et al.*, 2007] scales, respectively. Further details of flask sampling can be found in the auxiliary materials.[1]

3. Methodology

[6] The LPDM employed in our work is the Stochastic Time Inverted Lagrangian Transport (STILT) model, run in the time-reversed (receptor-oriented) mode. STILT has been developed and applied to regional emission of CO_2 previously, as described by *Lin et al.* [2003], *Gerbig et al.* [2003], and *Matross et al.* [2006].

3.1. Meteorological Input and Footprint Estimation

[7] We drove STILT with meteorological fields from the Weather Research and Forecasting (WRF) model [*Skamarock et al.*, 2005]. We modified WRF to output time-averaged mass fluxes (rather than instantaneous advective velocities) to drive STILT, which results in very good mass conservation (a critical consideration for surface flux estimates), and we also obtained WRF convective mass fluxes that are used directly in STILT. We employed 40-km resolution in WRF version 2.2 that includes analysis nudging to improve meteorological realism. Effects of turbulence in the Planetary Boundary Layer are represented as a Markov chain process in STILT [*Lin et al.*, 2003].

[8] Given input meteorological data, the STILT model transports ensembles of 100 particles (air parcels) backwards in time 6 days for the set of ~300 receptor points; advecting particles further back in time increases the fraction of particles to reach the boundary, but going beyond 6 days has no effect on the footprint, and an insignificant effect on boundary values of the gases considered here. For each receptor, we calculate the footprint, which represents the sensitivity of the receptor point to surface sources, in units of ppb/(μmol m^{-2} s^{-1}). The footprint is calculated by counting the number of particles in a surface-influenced region (defined as ½ of the estimated PBL height [*Gerbig et al.*, 2003]) and the time spent in the region (for details, see *Lin et al.* [2003]). The footprint is multiplied by an *a priori* emission field to compute the associated contribution to the mixing ratio at the receptor.

3.2. Emissions Inventories

[9] We need to represent sources and sinks that affect atmospheric concentrations on regional spatial and temporal scales. For CH_4, we include natural wetland and anthropogenic sources in our *a priori* emission estimates. Wetland sources are given by the 'JK' wetland inventory described by *Bergamaschi et al.* [2007], indexed on a ½° × ½° grid and changing monthly. Anthropogenic sources are from the EDGAR 32FT2000 inventory [*Olivier et al.*, 2005] (available on a 1° × 1° grid, constant in time). See Figure 1b for spatial distribution of emissions.

[10] For N_2O, two different inventories are used, EDGAR 32FT2000 and GEIA [*Bouwman et al.*, 1995]. EDGAR includes all anthropogenic sources of N_2O, but does not include natural sources. GEIA includes both natural and anthropogenic sources. Both N_2O inventories are held constant in time and are available on 1° × 1° grids. See Figure 1c for spatial distribution of EDGAR emissions.

[11] Emissions categories for GEIA include soils (natural and agricultural), animal excreta, post-forest clearing en-

[1] Auxiliary materials are available in the HTML. doi:10.1029/2008GL034031.

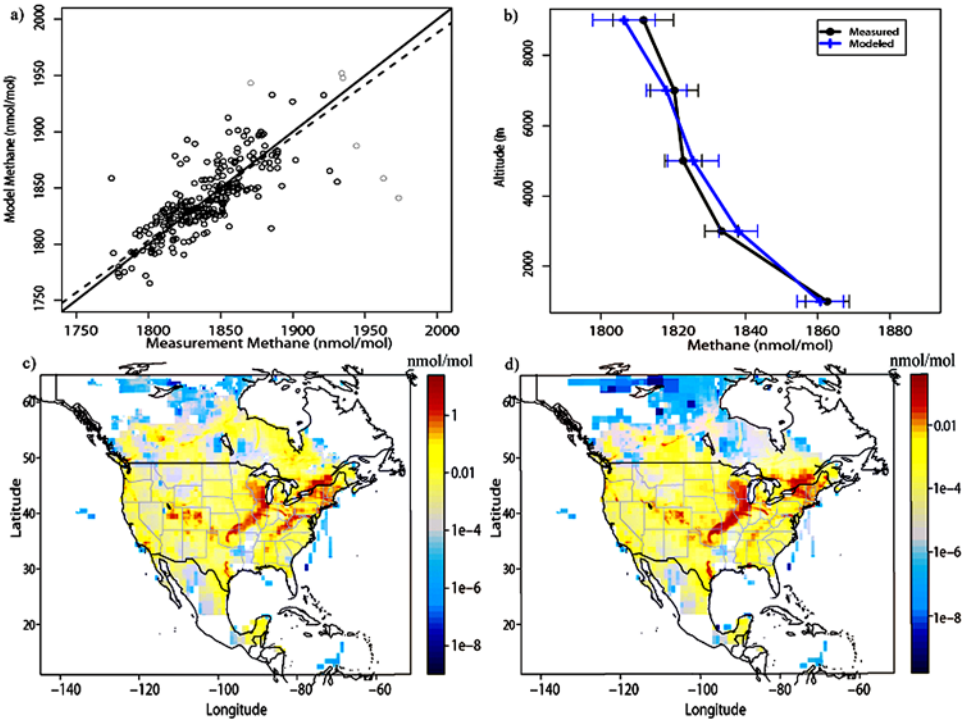

Figure 2. (a) Model vs. measurement for CH_4, solid line is 1:1 line, dashed line is fit. Grayed points are outliers not included in fit (>3σ from the mean). (b) Bin-averaged vertical distribution showing scaled model in blue, and measurements in black, whiskers illustrate 95% confidence intervals. (c) Total mission footprint multiplied by CH_4 emissions, showing surface contribution to receptor points. (d) Surface contribution of N_2O to receptor points.

hanced soil emissions, agricultural waste burning, biofuels, fossil fuels, industrial sources, and ocean emissions. EDGAR categories for both CH_4 and N_2O include fossil fuels, biofuels, industrial sources, agricultural sources, and waste handling. Seasonal factors for the different source categories in EDGAR exist for testing purposes, but the majority of the sources considered here do not exhibit strong temporal variation, and large uncertainty exists in these estimates, so they are not included. The exception is agricultural emissions of N_2O, and seasonal factors are considered here as discussed in section 4.2.

3.3. Upwind Boundary Condition

[12] To compare with measurements, the mixing ratio enhancements due to surface fluxes must be added to a background mixing ratio advected from the domain boundary. We retrieve background mixing ratios from a two-dimensional (latitude, height), temporally-varying array placed at 145°W longitude. Mixing ratios are attributed to particles as they cross this boundary. If particles do not reach the boundary, they are given a background mixing ratio taken from the 145°W boundary at the same latitude and altitude as the particle location 6 days traveled back in time. For CH_4, TM3 "scenario one" model output as described by *Houweling et al.* [2006] is used for the boundary, shifted down by 27 nmol/mol. This bias is found by comparing model with COBRA-NA measurements above 3km where surface emissions are found to have minimal influence on weekly timescales (on average less than 5 nmol/mol, for methane). It is also consistent with the known offset of ~20 nmol/mol found by *Houweling et al.* [2006].

[13] Neither data nor global model results are available to set a boundary condition for N_2O. We plotted the observed N_2O vs. CH_4 above 3km, where surface influence is small, to determine the ratio of N_2O variations vs. CH_4 at the boundary (0.010). We then multiplied the CH_4 boundary values by this factor and added the relevant intercept, 299.8 nmol/mol. Using our prior fluxes, variation in background is responsible for 57% of the variation for methane, and 50% of the variation for nitrous oxide.

3.4. Assessment/Optimization Approach

[14] We fit model results to observations including uncertainty in both x and y, using the χ^2 (fitexy) method of *Press et al.* [1992], to ensure unbiased fit parameters [*Miller and Tans*, 2003]. We assume that errors in the prior sources are constant in space and time, and find one scaling factor (inverse of the fit slope) for the entire emissions field, providing a simple and straightforward approach to assess model performance and determine the North American budgets. We do not have sufficient data to decouple different source-types or to examine inventory errors in smaller spatial regions. The intercept of the fit, representing a correction to the boundary condition, has little or no effect on the scaling factor. Further information on the effect of the boundary, chi-square optimization, and uncertainties (including footprint bias), is given in the auxiliary materials.

4. Results and Discussion

4.1. Methane

[15] Results for CH_4 are remarkable in the point-by-point agreement between simulated and measured mixing ratios

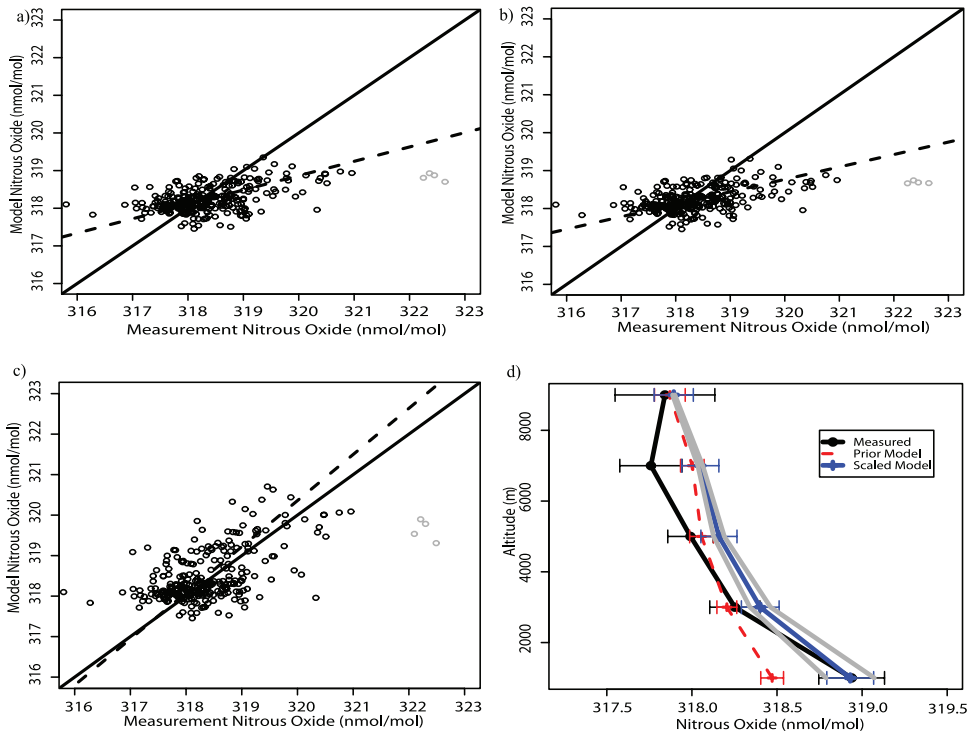

Figure 3. (a) Model vs. measurement for N_2O, EDGAR case, solid line is 1:1 line, dashed line is fit. Grayed points are outliers not included in fit (>3σ from the mean) (b) GEIA case. (c) EDGAR case scaled by found multiplier (2.62). (d) Binned vertical distribution showing un-scaled model (EDGAR case) in red, scaled model in blue, scaled model with upper and lower bounds on scaling factor in gray, and measurements in black, whiskers illustrate 95% confidence intervals.

(Figures 2a and S1b), with a fitted slope remarkably close to one (0.924 ± 0.13), implying a scaling factor for the inventory of 1.08 ± 0.15 (note potential unaccounted footprint bias may expand the uncertainty). Applying the scaling factor to the emissions gives the vertical distribution illustrated in Figure 2b; the very good agreement suggests that the WRF-driven STILT model is able to accurately connect measurement locations with source regions upstream, and thus to faithfully model the vertical distribution of CH_4 in the atmosphere—a critical indicator of surface emissions. The agreement above 3km indicates that the advected boundary condition is sufficiently accurate for our purposes. The fidelity of the model to the observations also suggests accuracy in the spatial distribution of the prior emissions inventory, though potentially cancelling errors or footprint bias cannot be ruled out (discussed further in the auxiliary materials). Anthropogenic sources dominate the inventory in the region that we sampled: fossil fuels, waste handling, and agriculture produce 97% of the total modeled enhancement. Natural wetlands are hardly represented (< 3% total modeled enhancement) in our measurements, and so our assessment of the inventory is restricted to anthropogenic emissions. Spatially, we are sensitive to the high emissions regions in the northern Midwest and Northeast, but not to the large emissions from the gulf coast region (Figure 2c).

4.2. Nitrous Oxide

[16] Results for N_2O are shown in Figure 3. Simulations based on the GEIA and EDGAR inventories are very similar, with both simulations underestimating atmospheric measurements. Fitting model vs. EDGAR yields a slope of 0.381 ± 0.072 and vs. GEIA a slope of 0.328 ± 0.065. Increasing emissions by factors of 2.62 ± 0.50 and 3.05 ± 0.61 for EDGAR and GEIA, respectively, improves model-measurement agreement in the shape of the vertical profile (see Figures 3c and 3d for the EDGAR inventory). The offset above 3km is likely caused by the upwind boundary condition. Though the slope from the 1km to 3km bin appears somewhat steeper in the measurement than the model, the upper error bound on the scaling, seen in gray, nearly captures the same trend. There is a potential that vertical mixing errors could bias the analysis, though the methane results suggest otherwise. A more likely cause is the advected boundary condition, though consistency between model and measurement, when considering error bounds, suggests the effect on our analysis is small. Spatially, we have coverage of the strong emissions regions through the Midwest and the Northeast (Figure 2d).

[17] These results indicate that in early summer current inventories give N_2O emissions too low by a factor of 2–3 for much of the USA and southern Canada. Since agricultural emissions dominate the source signal, seasonality may explain some of the under-representation. But applying the published seasonal factors from EDGAR would actually worsen agreement, as the scaling factor for May and June is 0.85. However, the peak scaling factor, for March, is 2.35. If agricultural emissions peaked in May–June instead of March, then our results would be consistent with the EDGAR inventory scaled by this earlier seasonal peak,

and the overall annual emissions might not be higher by the indicated factor.

5. Conclusion

[18] This study simultaneously estimated continental-scale surface fluxes of two important greenhouse gases, CH_4 and N_2O, using a top-down approach built upon the STILT LPDM, constrained by collocated atmospheric measurements from aircraft and optimized with a simple regression approach. Results suggest the EDGAR inventory for CH_4 accurately accounts for emissions over much of the U.S. and southern Canada (accurate to 8 ± 14%). In contrast, N_2O emissions in both EDGAR and GEIA are underestimated (by factors of 2.62 ± 0.50 and 3.05 ± 0.61, respectively). Potential footprint bias may expand uncertainty but we believe this effect to be small (see auxiliary materials). Seasonality in agricultural emissions could be responsible for the discrepancy. However, if seasonality does not explain the under-representation in future studies, this underestimate would have important consequences for predictions of climate change, given the strong radiative forcing by N_2O. If these scaling factors applied uniformly over the USA and Canada, then the yearly anthropogenic contribution of these countries to global emissions would be 49 Tg CH_4 and 4.3 Tg N_2O. Extending this approach with measurements covering at least one full year would provide valuable information on the seasonality of emissions. The two main potential sources for bias in this approach, the upwind boundary condition and transport error, could be further quantified and reduced with measured vertical profiles along the boundary, and analysis with gases such as SF_6, respectively.

[19] **Acknowledgments.** Work at AER has been supported by the NASA Terrestrial Ecology Program. E.A.K. acknowledges financial support from the Department of Defense through the NDSEG fellowship program. COBRA-2003 was funded by the NASA Large Scale Biosphere-Atmosphere Experiment in Amazonia (NASA NCC5-590), by NASA support to J.B.M. and B.B.S. (NAG5-11430), and through the NOAA Office of Oceanic and Atmospheric Research. We also thank Ed Dlugokencky and Patricia Lang for analysis and quality control of all CH_4 and N_2O data. The National Center for Atmospheric Research is sponsored by the National Science Foundation.

References

Bergamaschi, P., et al. (2007), Satellite chartography of atmospheric methane from SCIAMACHY on board ENVISAT: 2. Evaluation based on inverse model simulations, *J. Geophys. Res.*, *112*, D02304, doi:10.1029/2006JD007268.

Bouwman, A. F., K. W. van der Hoek, and J. G. J. Olivier (1995), Uncertainties in the global source distribution of N_2O, *J. Geophys. Res.*, *100*(D2), 2785–2800.

Chen, Y.-H., and R. G. Prinn (2006), Estimation of atmospheric methane emissions between 1996 and 2001 using a three-dimensional global chemical transport model, *J. Geophys. Res.*, *111*, D10307, doi:10.1029/2005JD006058.

Dlugokencky, E. J., R. C. Myers, P. M. Lang, K. A. Masarie, A. M. Crotwell, K. W. Thoning, B. D. Hall, J. W. Elkins, and L. P. Steele (2005), Conversion of NOAA atmospheric dry air CH_4 mole fractions to a gravimetrically prepared standard scale, *J. Geophys. Res.*, *110*, D18306, doi:10.1029/2005JD006035.

Gerbig, C., J. C. Lin, S. C. Wofsy, B. C. Daube, A. E. Andrews, B. B. Stephens, P. S. Bakwin, and C. A. Grainger (2003), Toward constraining regional-scale fluxes of CO_2 with atmospheric observations over a continent: 2. Analysis of COBRA data using a receptor-oriented framework, *J. Geophys. Res.*, *108*(D24), 4757, doi:10.1029/2003JD003770.

Gimson, N. R., and M. Uliasz (2003), The determination of agricultural methane emissions in New Zealand using inverse modeling techniques, *Atmos. Environ.*, *37*, 3903–3912.

Hall, B. D., G. S. Dutton, and J. W. Elkins (2007), The NOAA nitrous oxide standard scale for atmospheric observations, *J. Geophys. Res.*, *112*, D09305, doi:10.1029/2006JD007954.

Hirsch, A. I., A. M. Michalak, L. M. Bruhwiler, W. Peters, E. J. Dlugokencky, and P. P. Tans (2006), Inverse modeling estimates of the global nitrous oxide surface flux from 1998–2001, *Global Biogeochem. Cycles*, *20*, GB1008, doi:10.1029/2004GB002443.

Hofmann, D. J., J. H. Butler, E. J. Dlugokencky, J. W. Elkins, K. Masarie, S. A. Montzka, and P. Tans (2006), The role of carbon dioxide in climate forcing from 1979–2004: Introduction of the annual greenhouse gas index, *Tellus, Ser. B*, *58*, 614–619.

Houweling, S., T. Röckmann, I. Aben, F. Keppler, M. Krol, J. F. Meirink, E. J. Dlugokencky, and C. Frankenberg (2006), Atmospheric constraints on global emissions of methane from plants, *Geophys. Res. Lett.*, *33*, L15821, doi:10.1029/2006GL026162.

Hurst, D. F., J. C. Lin, P. A. Romashkin, B. C. Daube, C. Gerbig, D. M. Matross, S. C. Wofsy, B. D. Hall, and J. W. Elkins (2006), Continuing global significance of emissions of Montreal Protocol–restricted halocarbons in the United States and Canada, *J. Geophys. Res.*, *111*, D15302, doi:10.1029/2005JD006785.

Lin, J. C., C. Gerbig, S. C. Wofsy, A. E. Andrews, B. C. Daube, K. J. Davis, and C. A. Grainger (2003), A near-field tool for simulating the upstream influence of atmospheric observations: The Stochastic Time-Inverted Lagrangian Transport (STILT) model, *J. Geophys. Res.*, *108*(D16), 4493, doi:10.1029/2002JD003161.

Matross, D. M., et al. (2006), Estimating regional carbon exchange in New England and Quebec by combining atmospheric, ground-based and satellite data, *Tellus, Ser. B*, *58*, 344–358.

Miller, J. B., and P. P. Tans (2003), Calculating isotopic fractionation from atmospheric measurements at various scales, *Tellus, Ser. B*, *55*, 207–214.

Miller, J. B., L. V. Gatti, M. T. S. d'Amelio, A. M. Crotwell, E. J. Dlugokencky, P. Bakwin, P. Artaxo, and P. P. Tans (2007), Airborne measurements indicate large methane emissions from the eastern Amazon basin, *Geophys. Res. Lett.*, *34*, L10809, doi:10.1029/2006GL029213.

Nevison, C. D., N. M. Mahowald, R. F. Weiss, and R. G. Prinn (2007), Interannual and seasonal variability in atmospheric N_2O, *Global Biogeochem. Cycles*, *21*, GB3017, doi:10.1029/2006GB002755.

Olivier, J. G. J., J. A. Van Aardenne, F. Dentener, L. Ganzeveld, and J. A. H. W. Peters (2005), Recent trends in global greenhouse gas emissions: Regional trends and spatial distribution of key sources, in *Non-CO_2 Greenhouse Gases (NCGG–4)*, edited by A. van Amstel, pp. 325–330, Millpress, Rotterdam, Netherlands.

Press, W. H., S. A. Teukolsky, W. T. Vetterling, and B. P. Flannery (1992), *Numerical Recipes in FORTRAN: The Art of Scientific Computing*, 2nd ed., Cambridge Univ. Press, New York.

Prinn, R., D. Cunnold, R. Rasmussen, P. Simmonds, F. Alyea, A. Crawford, P. Fraser, and R. Rosen (1990), Atmospheric emissions and trends of nitrous oxide deduced from 10 years of ALE-GAGE data, *J. Geophys. Res.*, *95*(D11), 18,369–18,385.

Skamarock, W. C., J. B. Klemp, J. Dudhia, D. O. Gill, D. M. Barker, W. Wang, and J. G. Powers (2005), A description of the advanced research WRF version 2, *Tech. Note 468+STR*, 88 pp., Natl. Cent. for Atmos. Res., Boulder, Colo.

Stohl, A., C. Forster, S. Eckhardt, N. Spichtinger, H. Huntrieser, J. Heland, H. Schlager, S. Wilhelm, F. Arnold, and O. Cooper (2003), A backward modeling study of intercontinental pollution transport using aircraft measurements, *J. Geophys. Res.*, *108*(D12), 4370, doi:10.1029/2002JD002862.

B. C. Daube, Department of Earth and Planetary Sciences, Harvard University, 20 Oxford Street, Cambridge, MA 02138, USA.

J. Eluszkiewicz and T. Nehrkorn, Atmospheric and Environmental Research, Inc., 131 Hartwell Avenue, Lexington, MA 02421-3126, USA.

C. Gerbig, Max-Planck-Insitut für Biogeochemie, P.O. Box 10 01 64, D-07701 Jena, Germany.

S. Houweling, Netherlands Institute for Space Research, Sorbonnelaan 2, NL-3584 CA, Utrecht, Netherlands.

J. O. Kaplan, Swiss Federal Institute for Forest, Snow, and Landscape Research, Station 2, CH-1015 Lausanne, Switzerland.

E. A. Kort, School of Engineering and Applied Sciences, Harvard University, Geomuseum 411, 24 Oxford Street, Cambridge, MA 02138, USA. (kort@fas.harvard.edu)

J. B. Miller, NOAA Earth System Research Laboratory, 325 Broadway, Boulder, CO 80305, USA.

B. B. Stephens, National Center for Atmospheric Research, 1850 Table Mesa Drive, Boulder, CO 80305, USA.

S. C. Wofsy, School of Engineering and Applied Sciences, Harvard University, Pierce Hall 110-D, 20 Oxford Street, Cambridge, MA 02138, USA.